ANALYSIS OF SECONDARY FLOW CHARACTERISTICS AND HYDRODYNAMIC INSTABILITY IN FLUID FLOW THROUGH CURVED DUCTS

Tilak T Chandratilleke*, Nima Nadim and Ramesh Narayanaswamy
*Author for correspondence
Department of Mechanical Engineering, Curtin University
GPO Box U1987
Perth WA6845
Australia,
E-mail: t.chandratilleke@curtin.edu.au

ABSTRACT

This paper presents an investigation on the unique flow characteristics associated with fluid flow through curved ducts, which are fundamentally different to those in straight fluid passages. In curved ducts, the flow is subjected to centrifugal forces that induce counter-rotating vortices in the main axial fluid stream and give rise to spiralling fluid motion, commonly known as secondary flow. The study develops a novel three-dimensional computational fluid dynamics analysis whereby the laminar developing fluid flow in a curved rectangular duct is modelled. The flow characteristics are identified for a range of flow rates and duct aspect ratios at several duct curvatures. The contours of secondary flow and axial velocities are obtained to recognise the influence of flow/geometrical parameters on the secondary flow. Comparisons are made between the numerical predictions and the available experimental data. It is observed that, with increased duct flow rate, the secondary flow intensifies and beyond a certain critical flow condition, leads to hydrodynamic instability. The fluid flow structure is then significantly altered with the appearance of additional pair (or pairs) of vortices, termed as Dean Vortices, at the outer wall of the curved duct. This flow behaviour is also highly influenced by the duct aspect (height to width) ratio. The paper develops and presents a new approach for predicting the onset of Dean vortex generation.

INTRODUCTION

Fluid flow through curved passages is a common occurrence in a vast range of industrial applications, such as in gas turbine blades, air conditioning, heat exchangers and rocket engine coolant passages. In a curved passage, centrifugal forces are developed in the flow due to channel curvature causing a counter rotating vortex motion applied on the axial flow through the passage. This creates characteristic spiralling fluid flow in the curved passage known as secondary flow. At a certain critical flow condition and beyond, additional pairs of counter rotating vortices appear on the outer concave wall of curved fluid passages. This flow condition is referred to as Dean's Hydrodynamic Instability and the additional vortices are known as Dean vortices, in recognition of the pioneering work in this field by Dean [1].

Dean [1] relates the secondary flow behaviour to a single parameter K, called the Dean number, which is defined as $K = \left[\frac{D_h}{R}\right]^{\frac{1}{2}} Re$. It has been identified that the Dean's instability is culminated through the interaction between the centrifugal forces and lateral fluid pressure gradient at the outer wall acting towards the duct centre of curvature. This instability has been illustrated with respect to duct velocity in the work of Moffat [2] and Eustice [3] who experimentally observed and verified the critical velocity requirements for Dean's instability.

White [4] performed flow visualisation on a coiled pipe and reported that, the flow curvature alters the laminar regime compared to straight channels allowing laminar-to-turbulent transition to occur at reduced flow velocities. Early analytical and experimental investigations, such as Baylis [5], Humphery et al [6], concluded that Dean number was solely responsible for secondary flow and Dean instability in curved passages. However later studies with curved rectangular ducts by Cheng et al [7], Ghia and Shokhey [8] and Sugiyama et al [9] have shown that the Dean instability is also dependent on the aspect ratio and curvature ratio along with the Dean number.

Literature reports many numerical studies among which some key studies are indicated below. Hoon et al [10] used a 2-dimensional numerical model for fluid and thermal behaviour in eccentric curved pipes and discussed the relationship among Dean number, friction factor and Nusselt number in the range $0 \leq K \leq 900$ and Grashof $12.5 \leq Gr \leq 12500$. Yamamaoto et al [11] numerically examined the flow field within a helical pipe and demonstrated the role of centrifugal forces in the formation

of secondary flow. Ko et al. used flow entropy generation as a technique to identify secondary flow instability and performed thermal optimisation on rectangular passages in both laminar and turbulent regimes [12,13,14].

Chandratilleke et al [15,16,17] report an extensive parametric study examining the effects of curvature ratio and aspect ratio as well as the wall heat flux. The validation of numerical work has been performed against their own experimental data [15,16]. Their numerical method, that was effectively a 2-dimensional formulation, used toroidal coordinates and utilised a stream function approach with dynamic similarity in axial direction. Intersecting stream function contours were deployed as a qualitative criterion for detecting occurrence flow instability and Dean vortices. This approach is clearly adequate for 2-dimensional flow systems and cannot be extended for real flow situations. They discussed results in a comprehensive range of Dean number $25 \leq K \leq 500$, aspect ratio $1 \leq Ar \leq 8$ and Grashof number $12.5 \leq Gr \leq 12500$. It has been illustrated that the onset of Dean instability would vary with the duct aspect ratio and curvature ratio while the application of wall heat flux radically changes the flow patterns. Subsequently, other numerical work such as those carried out by Yanase [18] and Fellouah et al [19,20] have validated the results of Chandratilleke et al [16].

Most published work focus on 2-dimenasional numerical models. Accurate 3-dimensional simulations are clearly scarce in literature largely due to the computational complexities arising from secondary flow perturbations superimposed on the main axial flow through curved passages. H. Fellouah et al [19,20] have attempted to developed an elementary 3-dimensional simulation covering duct curvature ratios of $5.5 \leq \gamma \leq 20$ and aspect ratios of $0.5 \leq Ar \leq 12$. With water and air as working fluids, this model showed reasonable agreement with their own experiments involving a semi-circular channel test section that permitted visualisation of vortex formation along channel locations for various Dean numbers. They presented a quantitative criterion for identifying the Dean instability in curved channels using the radial gradient of the axial velocity in channels. Secondary flow dynamics suggest inadequacy of this approach-it is not the axial flow velocity in channel but the radial fluid velocity component directed towards outer wall is responsible for hydrodynamic instability and the stagnation pressure build-up at the outer curved wall.

The study presented in this paper develops a highly improved 3-dimensional computational model using helicity function that accurately describes the secondary flow vortex structures in the developing fluid flow through curved passages, thus overcoming limitations in mostly 2-dimensional previous studies. It incorporates a curvilinear mesh system for much compliant tracking of secondary flow path, facilitating more effective grid definition for capturing intricate details of vortex generation. In addition, a curvilinear coordinate system is defined along the outer duct wall permitting precise and efficient evaluation of local fluid pressure and its gradient in that vicinity. Simulation results are validated against the available experimental data. The study formulates and verifies a novel approach for computational schemes in identifying the onset of hydrodynamic flow instability in curved passages reflected by Dean vortex generation.

NOMENCLATURE

Ar	[-]	Aspect Ratio= a/b
a	[m]	Height of cross section
b	[m]	Width of cross section
D_h	[mm]	Hydraulic diameter = $\frac{2ab}{(a+b)}$
F_c	[N]	Centrifugal force
g	[m/s^2]	Gravity
H	[m/s^2]	Helicity ()
H^*	[m]	Dimensionless Helicity = $\frac{HD_h}{U_{in}^2}$
p	[Pa]	Static pressure
P^*		Dimensionless static pressure = $\frac{p}{\frac{1}{2}\rho U_{in}^2}$
K	[m]	Dean number = $\left(\frac{D_h}{R}\right)^{\frac{1}{2}} Re$
R	[m]	Radius of duct curvature
Re		Reynolds number = $\frac{U_{in} D_h}{\upsilon}$
$\vec{s}$	[m]	Coordinate along wall in duct cross section
U_{in}		Velocity at duct inlet (m/s)
u, v, w		Velocities component (m/s)
u^*, v^*, w^*		Dimensionless velocity = $\frac{u,v,w}{U_{in}}$
V_r	[m/s]	Axial velocity = $\sqrt{u^2 + w^2}$
x, y, z	[m]	Coordinates

Special characters

γ	[-]	Curvature ratio= R/b
θ	[Deg]	Angular position of cross section
υ	[m^2/s]	Kinematic Viscosity
μ	[Ns/m^2]	Dynamic viscosity
ρ	[kg/m^3]	Density
ω	[1/s]	Vorticity

Subscripts

c	centrifugal
h	hydraulic
in	inlet
r	axial

MODEL DESCRIPTION AND NUMERICAL METHOD

Fig. 1 illustrates the geometry used for the 3-dimensional model development. The model consists of a semi-circular curved duct fitted with straight inlet and outlet passages for ensuring fully developed flow at entry and smooth outflow at exit of curved duct. The working fluid air flows through the passage under steady and laminar flow conditions and, is assumed to be an incompressible Newtonian fluid. The analysis focuses on the curved duct that is designated by 0^o at inlet to 180^o at outlet. Fig. 1 also shows the coordinate system used, whose origin is pegged at curved duct outlet and the key geometrical parameters, duct height (a), width (b) and radius of curvature (R) considered in the study.

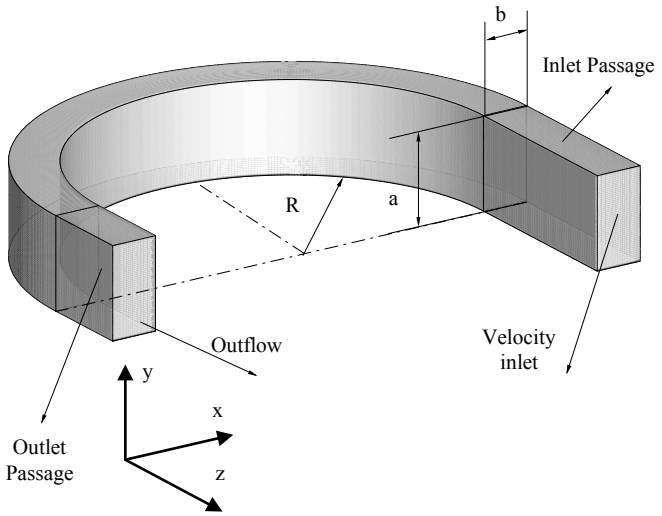

Figure 1 Geometry of computational model

The numerical model solves the following fundamental governing equations:

Time-averaged continuity equation;

$$\nabla . V = 0 \tag{1}$$

the momentum equations;

$$\rho V . \nabla V = -\nabla p + \mu \nabla^2 V + F_{Source} \tag{2}$$

and the centrifugal body force term,

$$F_c = \rho \frac{V_r^2}{r} = \rho \frac{(u^2 + w^2)}{\sqrt{x^2 + z^2}} \tag{3}$$

Incorporating the source term given by Equation (3), the momentum equations is re-written as,

$$u\frac{\partial u}{\partial x} + v\frac{\partial u}{\partial y} + w\frac{\partial u}{\partial z} =$$

$$\frac{1}{\rho}\frac{\partial p}{\partial x} + \nu\left(\frac{\partial^2 u}{\partial x^2} + \frac{\partial^2 v}{\partial y^2} + \frac{\partial^2 w}{\partial z^2}\right) + \frac{1 + sign(-z)}{2}\rho\frac{(u^2 + w^2)}{x^2 + z^2}x \tag{4}$$

$$u\frac{\partial v}{\partial x} + v\frac{\partial v}{\partial y} + w\frac{\partial v}{\partial z} = \frac{1}{\rho}\frac{\partial p}{\partial y} + \nu\left(\frac{\partial^2 u}{\partial x^2} + \frac{\partial^2 v}{\partial y^2} + \frac{\partial^2 w}{\partial z^2}\right) \tag{5}$$

$$u\frac{\partial w}{\partial x} + v\frac{\partial w}{\partial y} + w\frac{\partial w}{\partial z} =$$

$$\frac{1}{\rho}\frac{\partial p}{\partial z} + \nu\left(\frac{\partial^2 u}{\partial x^2} + \frac{\partial^2 v}{\partial y^2} + \frac{\partial^2 w}{\partial z^2}\right) + \frac{1 + sign(-z)}{2}\rho\frac{(u^2 + w^2}{x^2 + z^2}z \tag{6}$$

Here, a Sign Function is included to ensure the centrifugal source term is applied only for the curved section of the overall geometry (i.e. z ≤ 0). To be used with the dimensionless parameters, the characteristics length, velocity and pressure are chosen to be D_h, U_{in} and $\frac{1}{2}\rho {U_{in}}^2$, respectively.

In this 3-dimensional model, the flow patterns are described and examined by using the helicity function defined as,

$$H = V.\omega = u\left(\frac{\partial w}{\partial y} - \frac{\partial v}{\partial z}\right) + v\left(\frac{\partial u}{\partial z} - \frac{\partial w}{\partial x}\right) + w\left(\frac{\partial v}{\partial x} - \frac{\partial u}{\partial y}\right) \tag{7}$$

This is then non-dimensionalised as,

$$H \sim \frac{U_{in}^2}{D_h} \rightarrow H^* = H\frac{D_h}{U_{in}^2} \sim 1 \tag{8}$$

In evaluating the local fluid pressure gradient, a curvilinear coordinate $\vec{s}$ is defined along the outer duct wall boundary. This selection permits very accurate and convenient determination of the local pressure gradient $\frac{dp}{d\vec{s}}$ at the wall, and suitable even for irregular geometries of duct cross section. This gradient is defined as,

$$\frac{dp}{d\vec{S}} = \begin{cases} -\dfrac{dp}{dy} & y < 0 \\ \dfrac{dp}{dy} & y > 0 \end{cases} \tag{9}$$

Equation 9 incorporates a sign convention in accounting for the counter-rotating secondary vortex motion where positive sign represents the upper half of duct and negative sign the lower half. The pressure gradient is non-dimensionalised with the pressure and length reference parameters as,

$$\frac{dp^*}{d\vec{S}} = \begin{cases} -\dfrac{D_h}{1/2\,\rho U_{in}^2}\dfrac{dp}{dy} & y < 0 \\ \dfrac{D_h}{1/2\,\rho U_{in}^2}\dfrac{dp}{dy} & y > 0 \end{cases} \tag{10}$$

In solving the numerical model, a constant velocity condition is applied to the inlet of the straight duct section attached to the curved duct. The length of this inlet duct section is chosen to provide fully developed flow at entry to the curved duct section. A pressure outlet condition is applied to the outlet of the duct geometry. The air temperature is taken to be constant at 300 K over the entire solution domain. The duct walls are assumed to have no slip boundary condition. Table.1 provides the geometrical parametric range considered with the values of aspect ratio Ar and curvature ratio γ.

Table 1 Geometrical parametric range

A (mm)	B (mm)	R (mm)	Ar	γ
25	25	125	1	5
50	25	125	2	5
75	25	125	3	5
100	25	125	4	5
125	25	125	5	5
150	25	125	6	5

The solution is performed with respect to a suitably defined curvilinear mesh. In capturing the intricate characteristics of hydrodynamic instability, a progressively reducing mesh is considered in the analysis, facilitating a much finer mesh near the outer wall where the onset of instability is anticipated. This approach has not been attempted in previous studies [11-13,18-

19] arguing that a mesh size less than 1 mm did not sufficiently improve accuracy, but only led to increased computational time. The mesh refinement approach adopted in the current analysis clearly demonstrated that a finer mesh near the wall is critical for detecting the onset of Dean vortices as accurately as possible. For testing grid dependency, the study used five mesh schemes indicated in Table 2. In this, A is grid width and B is grid height in duct cross section, C is grid axial length along the duct and the factor D determines the progressive reduction in grid width over duct cross section.

Table 2 Parametric selection for mesh schemes

Scheme	Number of Grids			
	A	B	C	D
Mesh1	26	51	305	1
Mesh2	31	64	305	1
Mesh3	43	84	305	1
Mesh4	50	98	305	1
Mesh5	26	51	305	1.05

Fig. 2 illustrates the grid dependency test conducted using the velocity derivative in y-direction at the duct outer wall. It is clear that the Schemes 4 and 5 having mesh size less than 1 mm show much better suitability than the other three schemes. Nonetheless, Scheme 5 is taken to be the optimum because of its slightly larger cell volume arising from progressively varied mesh size. This approach provided a remarkable ability to capture the onset of vortex generation in the solution domain without causing excessive computational demand. As such, the present study performed all computations with Scheme 5 using mesh size less than 1 mm, hence achieving much higher accuracy than any previous reported work.

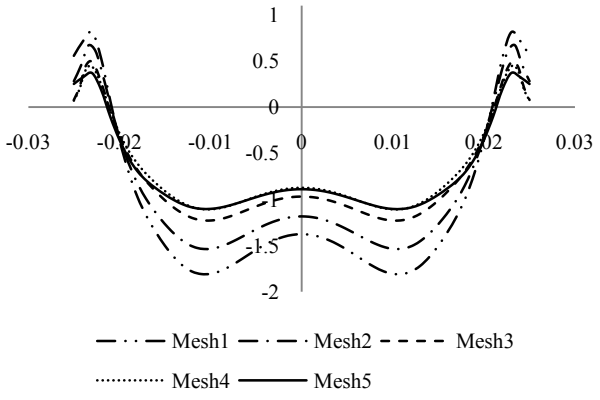

Figure 2 Grid independancy using with velocity derivative in y-direction at outer wall at curved duct exit, K=130, Ar=2

RESULTS AND DISCUSSION

Using the 3-dimensional numerical model developed, the air flow through a semi-circular curved rectangular duct of 25 mm width was analysed and the results were generated over an extensive range of geometrical and flow parameters. The duct height and the duct radius of curvature were varied, as given by table 1, to obtain the aspect ratio ar in the range of 1 to 6 and the curvature ratio γ in range of 3 to 13. Several fluid flow rates were chosen to achieve dean number k in the range of 80 to 380. This selection enables a direct comparison to be made with the available experimental data [17,19]. For analysis, the flow profiles were obtained at the exit plane (180^o position) of curved duct. The test cases indicating hydrodynamic instability were further refined by and running the simulations with much closer steps of k to establish the exact point of instability. This procedure was repeatedly applied for all permutations of aspect ratio and curvature ratio combinations whereby the critical dean number for each test case was ascertained.

For the purpose of validating results against published work, Fig. 3 shows the axial flow velocity in x and y directions predicted by the current 3-dimensional model and those from the 2-dimensional analyses of Ghia and Shokhey [8] and Fellouah et al [19]. It is seen that both magnitudes and trends of axial velocity are very favourably compared confirming the integrity of the numerical process.

Fig. 3 also illustrates the secondary flow effect on the axial fluid velocity in the curved passage. The profile (a) (along x axis) shows a skewed peak towards the outer wall arising from the centrifugal action and is characteristically different to axial velocity distribution in straight ducts. This peak gradually spreads towards the centre with increasing flow rate because of the radial pressure build at the outer wall. The profile on the right (along y axis) shows a dip in the centre and two marginal peaks on other side. These peaks essentially correspond to the upper and lower "eye" of secondary vortices (Fig. 4).

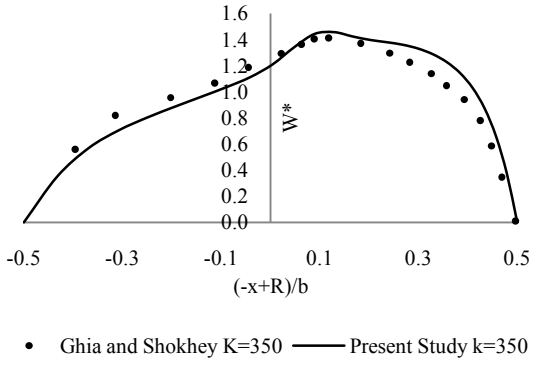

(a) At middle plane (y = 0) along x-axis

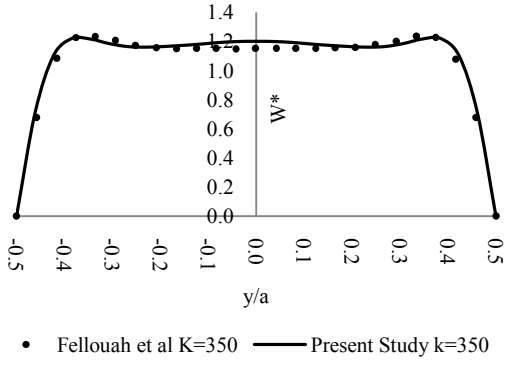

(b) At middle plane (x = R) along y-axis

Figure 3 Comparison of dimensionless axial velocity profile at curved duct exit plane, Ar=1

EFFECT OF FLOW RATE

A typical flow profile in terms of helicity contours in the curved duct cross section is shown in Fig. 4. The corresponding experimental flow pattern is also shown there for comparison. It is readily noted that these patterns are fundamentally different from those in straight channels. Even at low flow rates (or low K), the flow profile has two large counter-rotating vortices. This vortex flow is developed consequent to the centrifugal forces arising from the duct stream-wise curvature.

The centrifugal body forces due to the duct flow curvature essentially create two effects. It generates a positive radial fluid pressure field in the duct cross-section and induces a lateral fluid motion driven from inner duct wall towards outer duct wall (left-side wall in Fig. 4). This lateral fluid motion occurs against the radial pressure field generated by the centrifugal effect and is superimposed on the axial flow in the duct to create the secondary vortex flow structure. As the axial flow is increased (larger K), the lateral fluid motion becomes stronger and the radial pressure field is intensified. In the vicinity of the outer duct wall, the combined action of adverse radial pressure field and viscous effects slow down the lateral fluid motion and form a stagnant flow region. Beyond a certain critical value of K, the radial pressure gradient becomes sufficiently strong to reverse the flow direction of the lateral fluid flow. A weak local flow re-circulation is then established and an additional pair of vortices appears in the stagnant region near the outer wall. This flow situation is known as Dean Hydrodynamic Instability while the vortices are termed Dean Vortices. Typical helicity contours in the duct cross-section at hydrodynamic instability for K = 380 are shown in Fig. 4.

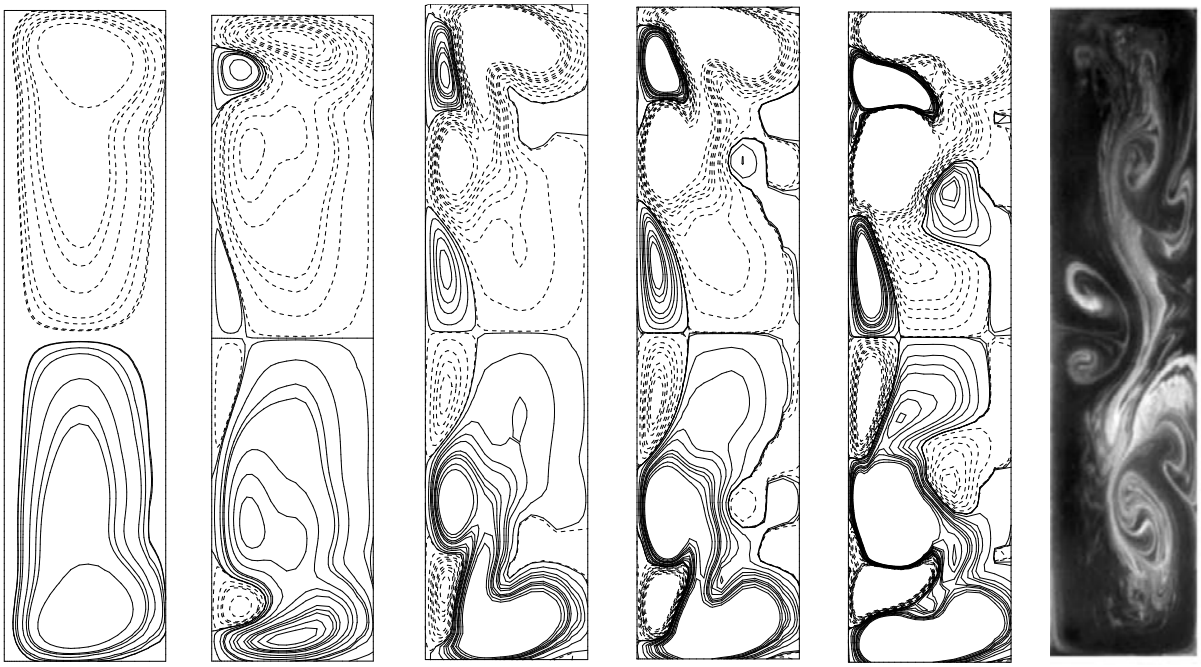

Figure 4 Helicity contours at different flow rates and experimental flow pattern [17], Ar = 4, $\gamma = 5$

DETERMINATION OF HYDRODYNAMIC INSTABILITY

Secondary flow Hydrodynamic Instability in curved passages is traditionally identified through tedious experimental flow visualisation techniques or by trial-and-error in numerical simulations. In the latter, repeated numerical computations are performed in the vicinity of anticipated flow conditions by continually narrowing the range to obtain the critical Dean number K and the flow patterns within the chosen tolerance limits. This involves guesswork and requires significant computational time. Chandratilleke et.al [16] successfully used the criterion of zero-potential stream function contours to identify locations of Dean vortex generation, which was practically sufficient for 2-dimensional simulations, but is not applicable for 3-dimensional flows. The work of Fellouah et al [19] used radial gradient of the axial velocity as a measure of identifying the flow instability. It is difficult for this selection to be rationalised because the axial velocity change in radial direction is not fundamentally connected with vortex generation. This inadequacy is clearly reflected in the work of Fellouah et al [19], where their simulation failed to detect the flow instability for some basic flow conditions. For example around K = 100, hydrodynamic instability is well observed in the current study, yet the analyses of Ghia and Shokhey [8] and Fellouah et al [19] did not identify this occurrence.

As of now, a reliable technique for detecting the hydrodynamic instability is not known in literature for 3-dimensional numerical simulations of flow through curved ducts. Formulation of a generalised approach is made further complicated by the dependency of pressure profile on the duct cross-sectional geometry. In addressing these issues, the current work reports for the first time, a reliable method for

identifying and predicting the hydrodynamic instability in curved fluid passages.

Based on the secondary flow vortex generation mechanism previously discussed, the study focuses on the outer wall fluid pressure profile as a key influencing parameter on hydrodynamic instability. The flow reversal leading to Dean vortex generation is fundamentally caused by the existence of adverse (positive) pressure gradient ($\frac{dp}{d\vec{s}} > 0$) at the outer duct wall in the direction of secondary fluid motion where $\vec{s}$ *is* the displacement variable in that direction of motion on the wall boundary. In ascertaining this, the pressure gradient profile along the outer wall is obtained.

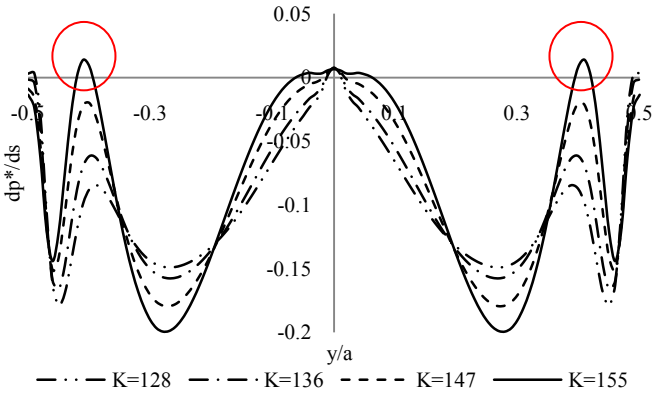

Ar=4, γ=5

Figure 5 Variation of dimensionless pressure gradient at the outer wall at duct exit (180°)

For a typical case, Fig. 5 shows the variation of pressure gradient $\frac{dp}{d\vec{s}}$ evaluated from Equations 9 and 10 along the outer duct wall for several chosen values of Dean number K. For low values of K, the pressure gradient remains negative over the entire outer wall. As K increases, the inflection points of the profile first acquire positive values for $\frac{dp}{d\vec{s}}$, creating (marked) regions of adverse pressure gradients at the outer wall. These localities develop flow reversal and represent critical conditions for hydrodynamic instability with Dean vortex generation. In Fig. 5, K = 155 is recognised to be the critical Dean number. This criterion based on adverse pressure gradient is presented as a reliable mechanistic technique to identify the onset hydrodynamic instability.

The effect of aspect ratio is demonstrated in Fig. 6 for a fixed curvature ratios of 4 and 5. It is noted that the critical Dean number initially increases with the duct aspect ratio and then falls away for higher K. This conforms to the previously reported experimental and numerical observations [7,16,18]. Fig.6 also shows a comparison of critical Dean number variation with aspect ratios predicted by present numerical model with the results of Chen et al [7]. It indicates good agreement although the current model predicts lower flow rates for setting off hydrodynamic instability.

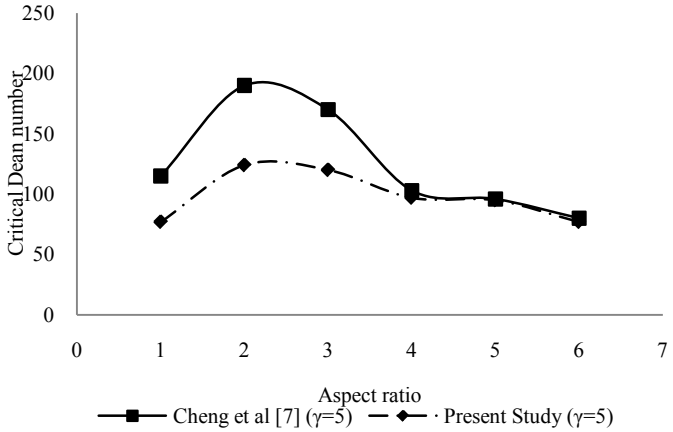

Figure 6 Variation of Critical Dean number with duct aspect ratio

In reported literature, the curvature ratio is defined in two versions, as R/b and R/D_h, without any rationale. In accommodating this, the variation of critical Dean Number with the duct curvature is illustrated in Fig. 7 in both versions.

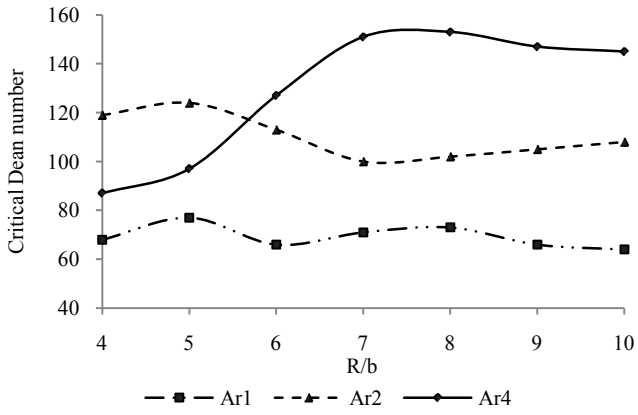

(a) With R/b

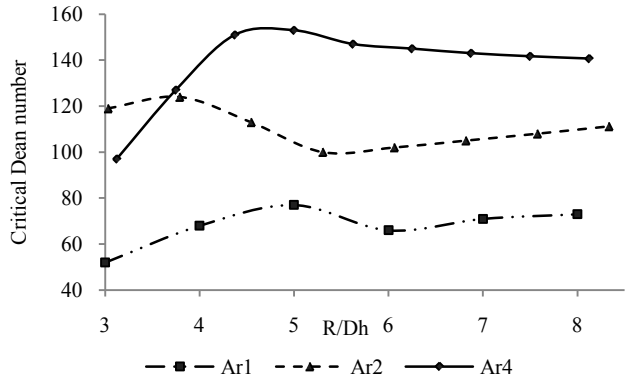

(b) With R/D_h

Figure 7 Variation of critical Dean with curvature ratio

The duct curvature directly influences the centrifugal body forces that generate secondary flow in curved ducts. A smaller curvature ratio (steep duct curvature) intensifies this effect

creating more vigorous secondary fluid motion. It therefore leads to hydrodynamic instability at lower flow rates. Conversely, a duct with larger curvature requires higher axial flow velocities to induce flow reversal, hence indicating a higher critical Dean Number. This behaviour is clearly reflected in Fig. 7. It is also noted that, for a given aspect ratio, the critical Dean Number shows a peak that is more pronounced and higher for ducts with large aspect ratios. This is attributed to fact that, in ducts of higher aspect ratio, the pressure distribution at the outer wall is more spread out and requires higher axial flow rate to trigger flow reversal at the outer wall. Within a range of aspect ratio up to about 10, the definition of curvature ratio shows a marginal impact.

CONCLUSIONS

The paper presents details of a novel 3-dimensional numerical simulation for secondary flow within curved ducts. It model incorporates helicity (vortex structures) function to account for realistic representation of secondary vortex flow and as such, the model shows a much improved approach than previously reported largely 2-dimensional studies. The analysis accurately predicts the flow behaviour in compliance with experimental and numerical work published in literature. The results generated examine the effects of fluid flow rate, duct aspect ratio and the duct curvature. For the first time in reported literature, the model presents a new analytical tool for determining the onset of hydrodynamic instability, which is based on adverse pressure gradient. This approach is shown to be accurate and reliable in identifying Dean vortex generation.

REFERENCES

[1] W.R. Dean, Fluid motion in a curved channel, *Proceedings of the Royal Society London,* Ser. A 121 (1928) 402–420.

[2] H.K. Moffatt, Viscous and resistive eddies near a sharp corner, *International Journal of Fluid Mechanics*, 48 (1) (1964) 1–18.

[3] J. Eustice, Experiments of streamline motion in curved pipes, Proc. Roy. Soc. London Ser. A 85 (1) (1911) 19–31.

[4] C.M. White, Streamline flow through curved pipes, *Proceedings of the Royal Society London,* Ser. A 123 (1929) 645–663.

[5] J.A. Baylis, Experiments on laminar flow in curved channels of square section, *International Journal of Fluid Mechanics,* 48 (3) (1971) 417–422.

[6] J.A.C. Humphrey, A.M.K. Taylor, J.H. Whitelaw, Laminar flow in a square duct of strong curvature, *International Journal of Fluid Mechanics,* 83 (1977) 509–527.

[7] K.C. Cheng, J. Nakayama, M. Akiyama, Effect of finite and infinite aspect ratios on flow patterns in curved rectangular channels, *Proceedings of the Flow Visualization International Symposium*, Tokyo, October 1977, p. 181.

[8] K.N. Ghia, J.S. Sokhey, Laminar incompressible viscous flow in curved ducts of rectangular cross-section, *Tranactions of ASME I: Journal of Fluids Engineering,* 99 (1977) 640–648.

[9] Sugiyama, Taro Hayashi, Koji Yamazaki, Flow Characteristics in the Curved Rectangular Channels, 1983, *Bulletin of JSME*, Vol.26, No.216, P532-552.

[10] Hoon Ki Choi, Seung O. Parkt, Mixed convection flow in curved annular ducts, *International Journal of Heat and Fluid Flow*, 1994, Vol. 37, No. 17, DD. 2761-2769.

[11] Kyoji Yamamoto, Md. Mahmud Alam, Junich Yasuhara, Agus Aribowo, Flow through a rotating helical pipe with circular cross-section, *International Journal of Heat and Fluid Flow*, 21 (2000) 213-220.

[12] Ko, T. H. Numerical investigation on laminar forced convection and entropy generation in a curved rectangular duct with longitudinal ribs mounted on heated wall. I*nternational Journal of Thermal Sciences*, 2005. 45: 390–404.

[13] Ko, T. H. A numerical study on entropy generation and optimization for laminar forced convection in a rectangular curved duct with longitudinal ribs. *International Journal of Thermal Sciences*, 2006, 45: 1113–1125.

[14] Ko, T. H.. A numerical study on entropy generation induced by turbulent forced convection in curved rectangular ducts with various aspect ratios. *International Communications in Heat and Mass Transfer*, 2008, 36: 25-31.

[15] T.T. Chandratilleke, Secondary flow characteristics and convective heat transfer in a curved rectangular duct with external heating, *Proceedings of 5th World Conference On Experimental Heat Transfer, Fluid Mechanics and Thermodynamics [ExHFT-5]*, Thessaloniki, Greece, September 24–28, 2001.

[16] T.T. Chandratilleke, Performance enhancement of a heat exchanger using secondary flow effects, *Proceedings of 2nd Pacific—Asia Conference in Mechanical Engineering,* Manila, Philippines, 9–11 September, 1998.

[17] Tilak T. Chandratilleke, Nursubiyakto, Numerical prediction of secondary flow and convective heat transfer in externally heated curved rectangular ducts. *International Journal of Thermal sciences* (2002), 42 187–198.

[18] S. Yanase, R. N. M., Y. Kaga, Numerical study of non-isothermal flow with convective heat transfer in a curved rectangular duct, *International Journal of Thermal Sciences*, 2005, 44 1047–1060.

[19] H. Fellouah, C. C., A. Ould El Moctar, H. Peerhossaini, A criterion for detection of the onset of Dean instability in Newtonian fluids, *European Journal of Mechanics B/Fluids*, 2006, 25: 505–531.

[20] H. Fellouaha, C. Castelainb, A. Ould-El-Moctarb, H. Peerhossaini, The Dean instability in power-law and Bingham fluids in a curved rectangular duct, *Journal of Non-Newtonian Fluid Mechanics*, 2010, 165, 163–173.